# Valence calculations of lanthanide anion binding energies: $6p$ attachments to $4f^n6s^2$ thresholds

Steven M. O'Malley and Donald R. Beck
*Physics Department, Michigan Technological University, Houghton, Michigan 49931, USA*
(Received 23 April 2008; published 25 July 2008)

Relativistic configuration-interaction calculations have been performed for anion states representing $6p$ attachments to all lanthanides with $4f^n6s^2$ ground states. The complexity of these systems requires a corelike treatment of the $4f$ subshell (same occupancy in all correlation configurations), and the methodology of creating *jls* restrictions on the $4f^n$ subgroup has been improved to include the mixing of *LS* terms from individual neutral *J* calculations. Results show a nearly linear decrease in electron affinity with $n$ for these lanthanides from 177 meV for $Pr^-$ ($n=3$) to 22 meV for $Tm^-$ ($n=13$).

DOI: 10.1103/PhysRevA.78.012510 PACS number(s): 32.10.Hq, 31.15.am, 31.15.ve, 31.15.vj

## I. INTRODUCTION

Over the last decade there has been renewed interest in lanthanide anions in the experimental community, though many laser photodetachment electron spectroscopy measurements [1–4] have produced electron affinities (EAs) of ~1.0 eV or higher, contradicting earlier accelerator mass spectrometry studies [5] with typical estimates of lanthanide EAs of ≥0.1 eV. We have presented possible explanations for these discrepancies by considering cases where photodetachment may be likely to leave the atom in an excited state [6,7] or where long-lived metastable states of the anion could be present [8,9]. A complete understanding of the photodetachment of each lanthanide would require extensive calculations of partial cross sections, including mixing of many channels with multiple resonance states, e.g., using the combined Fano-Mies theory [10,11] or the *R*-matrix method [12]. However, even limited treatment of photodetachment partial cross sections in our relativistic configuration-interaction (RCI) studies [6,7] has been a daunting task that has consumed the bulk of the operator and CPU time, compared to the *ab initio* binding energy (BE) calculations of each project.

In order to advance the overall understanding of the lanthanide anions as a whole, we have chosen to focus our attention on the BE calculations, specifically $6p$ attachments to $4f^n6s^2$ neutral ground states. In order to produce calculations of managable size, particularly near the center of the row, considerable *jls* restrictions of the $4f^n$ subgroup of electrons have been applied as described in detail in our recent $Nd^-$ work [7]. These approximations include treating the $4f$ subshells as corelike, i.e., correlating only the valence electrons (in this case a two-electron subgroup in each neutral atom and a three-electron subgroup in its anion). Our expectation is that the errors introduced affect all the $4f^n6s^26p$ states of an anion approximately equally, so that relative positioning of bound states and their *LS* composition is largely unaffected. Analysis of future experimental data that identifies individual photodetachment channels, e.g., anion ground state to a particular neutral threshold with a known energy [13], can then be used to shift all the RCI BEs of a given anion by a consistent amount to provide improved values for BEs of excited states. Additionally, by treating all these systems with the same amount of correlation (types of configurations and saturation of basis sets) it is expected that future corrections to a few of these anions may also be used to improve estimates of the remaining $4f^n6s^26p$ lanthanide states by scaling of the data presented here.

## II. METHODOLOGY

### A. One-electron wave functions

Our one-electron radial wave functions are generated by the multiconfigurational Dirac-Fock (MCDF) code of Desclaux [14]. The neutral calculations include $4f^n(6s^2+6p^2+5d^2)$ with $4f^n5d6s$ excluded due to negligible mixing with the $4f^n6s^2$ manifold. The anion radial wave functions are generated using all three $4f^n(5d+6s)^26p$ configurations plus $4f^n6p^3$. The purity of the anion states in terms of $6p_{1/2}$ vs $6p_{3/2}$ attachment to $4f^n6s^2J=J_n$ neutral ground states is >90%, and the dominant $6p$ radial wave function for each optimized level is much more diffuse than its counterpart (>7.4 a.u. vs ~5.5 a.u.). Intermediate level calculations show that simultaneous optimization of multiple levels of a given anion *J* is best achieved by hybrid one-electron basis sets that "swap out" the more compact $6p$ and $5d$ radial wave functions between calculations optimized to levels representing alternate attachments (in these cases the $J_n+1/2$ and $J_n+3/2$ bases are blended as are those of $J_n-1/2$ and $J_n-3/2$).

Valence subshells not occupied in the MCDF configurations are represented by screened hydrogenic "virtual" orbitals, denoted $vl$. The effective charge, $Z^*$, of each virtual radial wave function is determined via energy minimization within the RCI calculations.

### B. Many-electron wave functions

Our many-electron basis functions are eigenstates of $J^2$, $J_z$, and parity and are constructed of linear combinations of antisymmetrized determinants of the one-electron basis functions. Correlation in the neutral calculations consists of single and double replacements within the $6s^2$ subgroup restricted to $j\leq 4$ (the maximum $j$ of the $6s^2\rightarrow 6p^2+5d^2$ configurations which represent ~3.8% of the RCI wave function and ~95% of the correlation energy). In the anion calculations similar restrictions are applied to single and double replacements within the $6s^26p$ subgroup with the $j$

 

restrictions chosen also to correlate the important $4f^n(5d6s6p+5d^26p+6p^3)$ configurations which have typical mixing of 3%–6%, 0.5%–1.5%, and 1%–3%, respectively. In anticipation of increased complication of RCI calculations of mid-row lanthanides over our recent $Nd^-$ ($n=4$) work [7], the one-electron basis sets were restricted to $l=3$ ($vf$) or less, and some computationally expensive second order (with respect to $4f^n6s^26p$) correlation configurations, such as $4f^n5d^2vf$ and $4f^n5dvdvf$, were omitted. This trimming of the RCI bases results in a reduction of the total determinants by >40% with relative energy losses of only 2–3 meV.

### C. $4f^n$ *jls* restrictions

Our initial approach to these $4f^n6s^26p$ calculations [7] was to restrict the $4f^n$ subgroup to the dominant *LS* term of the neutral ground state (*LS* purity of all the lanthanide $4f^n6s^2$ ground states is >90% [13]). Recently, we have expanded the methodology to allow a rotation of the bases within the $4f^n$ subgroup to match the *jls* composition to intermediate level RCI neutral *JLS* calculations. For example, in Pr ($n=3$) the ground state and first few excited states are primarily $^4I_{9/2,11/2,13/2,15/2}$ [13] with secondary mixing (1%–2%) of $^2H_{9/2,11/2}$ or $^2K_{13/2,15/2}$. The $4f^3$ subgroup in all Pr and $Pr^-$ configurations therefore contains four basis functions with the *ls* composition for each $j=9/2,11/2,13/2,15/2$ matching the *LS* composition of the lowest level of the neutral calculation of the corresponding *J*. The result is a reduction in the number of RCI basis functions for every configuration, and the relative savings is larger the more complex the system (the closer it is to $n=7$). This approach does not result in fewer determinants, but in most cases the *L* and *S* of the neutral ground state are such that restriction to a single *LS* term would reduce this number by only a few percent. The exception is Eu ($n=7$), where $^8S$ and $^6P$ account for 99.98% of the $4f^76s^2J=7/2$ ground state's wave function. Retaining only these two *ls* terms in the subgroup mixing reduces the number of $4f^7$ determinants in this case by ~73% with essentially no impact on the $Eu^-$ BEs. The actual savings for each RCI basis member is more modest than the $4f^7$ subgroup itself, typically ~30%, due to the fact that application of the step-down operator (see below) creates many of the same individual determinants that would be produced by its application to some of the omitted $4f^7$ *ls* terms. Nevertheless, this restriction in the $Eu^-$ $n=7$ case combined with the fact that a $6p$ attachment to the $J=7/2$ Eu ground state makes a minimum $J=2$ (the number of determinants increases with decreasing *J*) means that the $Sm^-$ $J=1/2$ $n=6$ case actually becomes the most complex calculation presented here (~13 hours for the final basis set on a 2.4 GHz PC).

Once the appropriate *jls* mixing within the $4f^n$ subgroup is determined, a recently developed angular momentum addition code "pastes it together" with each of the necessary two- and three-electron subgroups. Part of this process requires use of the step-down operator on each of the two pieces of the wave function to create all possible $j_1m_1+j_2m_2$ combinations that make each desired total *J*. While the initial time investment in preparing the input files for $Nd^-$ ($n=4$) [7] was several weeks (operator time, CPU time is a few seconds per file), the two- and three-electron input data could be used without modification for each new lanthanide in this study (only new data for each $4f^n$ subgroup was required). Additionally, automation of the process has ensured that for even the most complex cases, preparation time for the combined $(n+2)$- and $(n+3)$-electron basis functions for all the correlation configurations is at most one-half of a day on a 2.4 GHz PC.

### D. Impact of approximation techniques

To set the scope of the approximations made in these calculations into perspective, consider the case of $Eu^-$ which has final RCI bases sizes of ~1000 functions and ~1 M determinants (most other anions presented here have 4–5000 basis functions in the final calculation, since they have more than a single *j* for the $4f^n$ subgroup). Without restricting the $4f^7$ subgroup as described above, the number of basis functions is increased by a factor of 50, and the determinants are increased by a more modest factor of ~1.4 (the current basis size limit of $20k$ is thus already exceeded). Consider also the reintroduction of some minimally important, but computationally expensive, second-order effects and correlation involving $vg$ (and perhaps $vh$) subshells, both of which affect the BEs by at most a few meV. If all possible *j*'s of the $4f^7$ subgroup (rather than just $j=7/2$, the only allowed *j* of the $^8S$ dominant term) were also included, there would again be negligible impact on the BEs, but these expanded RCI calculations would then have ~$350k$ basis functions with ~3 M determinants (months of CPU time vs 5 hours, currently—assuming one could redimension the code to permit such a calculation). Similarly, attempting to include correlation involving the $4f$ subshell would potentially increase the complexity of these calculations by an order of magnitude while also injecting a host of other difficulties regarding proper positioning of configurations with $4f^n$, $4f^{n-1}$, and $4f^{n-2}$ subgroups without disruption of the valence correlation configurations. In short, the approximations discussed above are not a convenience but rather a necessity without which these mid-row lanthanide anion calculations could not currently be performed (even considering reasonable increases in computer power, say doubling or tripling the CPU speed and memory).

## III. RESULTS

### A. Anion level composition and BEs

Lanthanide anion $4f^n6s^26p$ BEs and level composition are presented in Table I. The *jls* rotation within the $4f^n$ subgroup discussed in Sec. II C precludes the use of pure *LS* basis functions in our final RCI calculations, however, projection onto complete basis sets of *LS* or other couplings is possible afterward. Here we present *LS* analysis with the levels grouped by total *J* (indicated in the leading *LS* term of each state) as well as a secondary analysis that indicates the *jj* coupling of the neutral core and the $6p$ electron, "$(j)$" and "$\{j\}$" denoting $6p_{1/2}$ and $6p_{3/2}$ attachments, respectively.

TABLE I. RCI *ab initio* BEs (meV) of $4f^n6s^26p$ lanthanide anion states. Both analyses are presented as percentages (rounded, with contributions of 1% or greater). The total $J$ of each state is given in the label of the leading $LS$ term, and the notations of the core $j$ in the $jj$ analysis, $(j)$ and $\{j\}$, indicate $6p_{1/2}$ and $6p_{3/2}$ attachments, respectively. The EA (ground state BE) for each ion is presented in bold numbers in the "BE" column. Values in the "Experiment" column represent EAs only, and cases with multiple experimental references are not necessarily aligned in the same row as the anion ground state.

| | | | | Other values | |
|---|---|---|---|---|---|
| Ion ($n$) | $LS$ composition | $jj$ attachment | BE | Experiment | Theory |
| $Pr^-$ (3) | $^5H_3$ 98, $^3G$ 2 | {9/2} 100 | 82 | | 4 [15] |
| | $^5I_4$ 66, $^3H$ 29, $^5H$ 4, $^1G$ 1 | (9/2) 92, {9/2} 8 | 161 | | 110 [15] |
| | $^3H_4$ 36, $^5H$ 34, $^5I$ 29, $^3G$ 1 | {9/2} 92, (9/2) 8 | 86 | | |
| | $^5K_5$ 77, $^3I$ 21, $^5I$ 1, $^3H$ 1 | (9/2) 99, {9/2} 1 | **177** | ⩾100 [5] | 128 [15] |
| | $^3I_5$ 40, $^5I$ 40, $^5K$ 17, $^5H$ 1, $^3H$ 1, $^1H$ 1 | {9/2} 98, (9/2) 1, (11/2) 1 | 100 | 962(24) [1] | |
| | $^3K_6$ 50, $^5K$ 45, $^5I$ 2, $^3I$ 2, $^1I$ 1 | {9/2} 97, (11/2) 2, {11/2} 1 | 85 | | 6 [15] |
| $Nd^-$ (4) | $^6H_{5/2}$ 99, $^4G$ 1 | {4} 100 | 84 | | 86 [7] |
| | $^4H_{7/2}$ 50, $^6I$ 41, $^6H$ 8, $^2G$ 1 | (4) 100 | 142 | | 144 [7] |
| | $^6I_{7/2}$ 50, $^6H$ 31, $^4H$ 18, $^4G$ 1 | {4} 100 | 73 | | 76 [7] |
| | $^6K_{9/2}$ 87, $^4I$ 12, $^4H$ 1 | (4) 94, {4} 6 | **167** | ⩾50 [5] | 169 [7] |
| | $^4I_{9/2}$ 47, $^6I$ 37, $^6K$ 7, $^6H$ 5, $^4H$ 3, $^2H$ 1 | {4} 94, (4) 5, {5} 1 | 63 | >1916 [4] | 66 [7] |
| | $^6K_{11/2}$ 51, $^4K$ 45, $^6I$ 2, $^4I$ 1, $^2I$ 1 | {4} 92, (5) 8 | 79 | | 81 [7] |
| | $^6K_{11/2}$ 41, $^4K$ 35, $^4I$ 18, $^6I$ 3, $^6H$ 1, $^4H$ 1, $^2I$ 1 | (5) 90, {4} 8, {5} 2 | 8 | | 6 [7] |
| $Pm^-$ (5) | $^7G_1$ 98, $^5F$ 2 | {5/2} 100 | 82 | | |
| | $^5G_2$ 62, $^7H$ 26, $^7G$ 10, $^3F$ 1, $^3F$ 1 | (5/2) 97, {5/2} 3 | 129 | | |
| | $^7G_2$ 48, $^7H$ 47, $^5G$ 4, $^5F$ 1 | {5/2} 94, {7/2} 3, (5/2) 3 | 58 | | |
| | $^7I_3$ 88, $^5H$ 10, $^5G$ 1, $^7H$ 1 | (5/2) 91, {5/2} 7, {7/2} 1, (7/2) 1 | **154** | | |
| | $^5G_3$ 34, $^7G$ 32, $^5H$ 23, $^7I$ 5, $^7H$ 4, $^5F$ 1, $^3G$ 1 | {5/2} 60, (7/2) 29, {7/2} 6, (5/2) 5 | 43 | | |
| | $^7H_3$ 69, $^5G$ 20, $^5H$ 9, $^7G$ 1, $^3F$ 1 | (7/2) 70, {5/2} 29, (5/2) 1 | 22 | | |
| | $^7I_4$ 75, $^5I$ 20, $^7H$ 2, $^5H$ 2, $^3H$ 1 | {5/2} 66, (7/2) 33, {7/2} 1 | 73 | | |
| | $^5I_4$ 59, $^5H$ 17, $^7I$ 17, $^5G$ 2, $^7H$ 2, $^7G$ 2, $^3H$ 1 | (7/2) 63, {5/2} 33, {7/2} 3, {9/2} 1 | 26 | | |
| $Sm^-$ (6) | $^8G_{1/2}$ 75, $^6F$ 12, $^6D$ 8, $^8F$ 4, $^4D$ 1 | (0) 87, (1) 9, {1} 3, {2} 1 | **130** | ⩾50 [5] | |
| | $^6D_{1/2}$ 57, $^8F$ 28, $^8G$ 13, $^4P$ 2 | (1) 87, (0) 11, {1} 2 | 88 | | |
| | $^8G_{3/2}$ 77, $^6F$ 10, $^6D$ 7, $^8F$ 5, $^8D$ 1 | (1) 87, {0} 7, (2) 3, {2} 1, {1} 1, {3} 1 | 95 | | |
| | $^8D_{3/2}$ 63, $^6D$ 21, $^8G$ 6, $^6F$ 4, $^6G$ 3, $^6P$ 2, $^8F$ 1 | {0} 57, (2) 18, {1} 17, (1) 5, {2} 3 | 53 | | |
| | $^8F_{3/2}$ 48, $^6D$ 32, $^8G$ 10, $^8D$ 9, $^4P$ 1 | (2) 71, {1} 17, {0} 6, {2} 3, (1) 3 | 16 | | |
| | $^6G_{3/2}$ 75, $^6F$ 10, $^8D$ 9, $^4F$ 3, $^8F$ 2, $^4D$ 1 | {1} 61, {0} 28, (2) 7, (1) 3, {3} 1 | 4 | | |
| | $^8G_{5/2}$ 85, $^8F$ 6, $^6F$ 6, $^6D$ 2, $^6G$ 1 | (2) 68, {1} 28, (3) 3, {2} 1 | 36 | | |
| | $^8D_{5/2}$ 48, $^6D$ 15, $^6F$ 14, $^6G$ 13, $^8F$ 8, $^6P$ 1, $^4F$ 1 | {1} 59, (2) 25, {2} 9, (3) 4, {3} 3 | 1 | | |
| $Eu^-$ (7) | $^7P_2$ 98, $^5P$ 1, $^5S$ 1 | {7/2} 100 | 5 | | |
| | $^9P_3$ 87, $^7P$ 12, $^7S$ 1 | (7/2) 97, {7/2} 3 | **117** | ⩾50 [5] | |
| | $^7P_3$ 88, $^9P$ 11, $^5P$ 1 | {7/2} 97, (7/2) 3 | 10 | 1053(25) [2] | |
| | $^9P_4$ 67, $^7P$ 32, $^7D$ 1 | (7/2) 93, {7/2} 7 | 104 | | |
| | $^7P_4$ 68, $^9P$ 31, $^5D$ 1 | {7/2} 93, (7/2) 7 | 17 | | |
| | $^9P_5$ 98, $^7D$ 2 | {7/2} 100 | 41 | | |

TABLE I. (*Continued.*)

| Ion ($n$) | $LS$ composition | $jj$ attachment | BE | Other values: Experiment | Other values: Theory |
|---|---|---|---|---|---|
| $Tb^-$ (9) | $^7G_7$ 46, $^5H$ 32, $^7H$ 18, $^5I$ 2, $^3I$ 1, $^7I$ 1 | (15/2) 99, {15/2} 1 | 78 | ⩾100 [5] | |
| | $^7H_8$ 59, $^5I$ 26, $^7I$ 13, $^3K$ 1, $^5K$ 1 | (15/2) 87, {15/2} 13 | **85** | >1165 [4] | |
| $Dy^-$ (10) | $^6H_{15/2}$ 58, $^4I$ 24, $^6I$ 14, $^4K$ 2, $^2K$ 1, $^6K$ 1 | (8) 100 | **63** | 15(3) [5] | |
| | $^6I_{17/2}$ 41, $^4K$ 40, $^6K$ 16, $^2L$ 2, $^4L$ 1 | (8) 97, {8} 3 | 62 | >0 [4] | |
| $Ho^-$ (11) | $^5H_7$ 71, $^3I$ 15, $^5I$ 13, $^3K$ 1 | (15/2) 98, {15/2} 2 | **50** | ⩽5 [5] | |
| | $^3K_8$ 51, $^5I$ 25, $^5K$ 20, $^3L$ 1, $^1L$ 1 | (15/2) 100 | 44 | | |
| $Er^-$ (12) | $^4G_{11/2}$ 79, $^4H$ 13, $^2H$ 8 | (6) 95, {6} 5 | **38** | ⩾5 [5] | |
| | $^2I_{13/2}$ 53, $^4I$ 30, $^4H$ 16, $^2K$ 1 | (6) 98, {6} 2 | 29 | | |
| $Tm^-$ (13) | $^3D_3$ 77, $^3F$ 18, $^1F$ 4, $^3G$ 1 | (7/2) 94, {7/2} 6 | **22** | 32(7) [5] | 27–136 [16] |
| | $^3G_4$ 45, $^1G$ 41, $^3F$ 14 | (7/2) 98, {7/2} 2 | 14 | 1029(22) [3] | |

The reference to our own $Nd^-$ work [7] is less than 1 year old, but we have presented updated data here to illustrate the subtle improvements in the $4f^n$ *jls* restrictions. The differences of 2–3 eV in the BEs are due to the trimming of the bases that removed >40% of the determinants with minimal energy losses as discussed in Sec. II B. Note the presence of ~1% mixing of doublet terms in some of these $Nd^-$ levels due to a similar amount of mixing of $^3H$ in the $^5I$ neutral thresholds [13] (only quartets and sextets are possible using the single-term algorithm). While the prior calculations relied on shifting of BEs for attachments to excited neutral thresholds to account for differing $LS$ purity of the neutral cores [13], the improved $4f^n$ *jls* restrictions ensure a more accurate relative position of these states within the RCI anion calculations. This effect is important in nearly degenerate cases such as the $^5G_3$ and $^7H_3$ levels of $Pm^-$ which are primarily attachments to the $4f^5 6s^2$ $J=5/2$ ground state and the $J=7/2$ first excited state, respectively, though the $jj$ analysis indicates mixing of ~30% between the two. The single-term *jls* restrictions would require a shifting of the $^7H_3$ energy after the fact, likely producing the same BE to within a few meV but less accurate composition due to the uncorrected relative position of the two levels within the RCI calculation.

The differences in BEs for these $Pr^-$ values and our group's earlier RCI calculations [15] are due primarily to the fact that the $4f^3$ *jls* restrictions allow much more correlation in the valence three-electron subgroup, with little increase in the total basis size (~3800 functions vs ~3000 in the earlier calculations). Even for $n=3$, the *jls* restrictions to one basis function per $j$ of the $4f^n$ subgroup is a significant reduction from 7, 5, 3, and 3 functions for each of $j=9/2$ through $j=15/2$ (though the earlier work did remove the

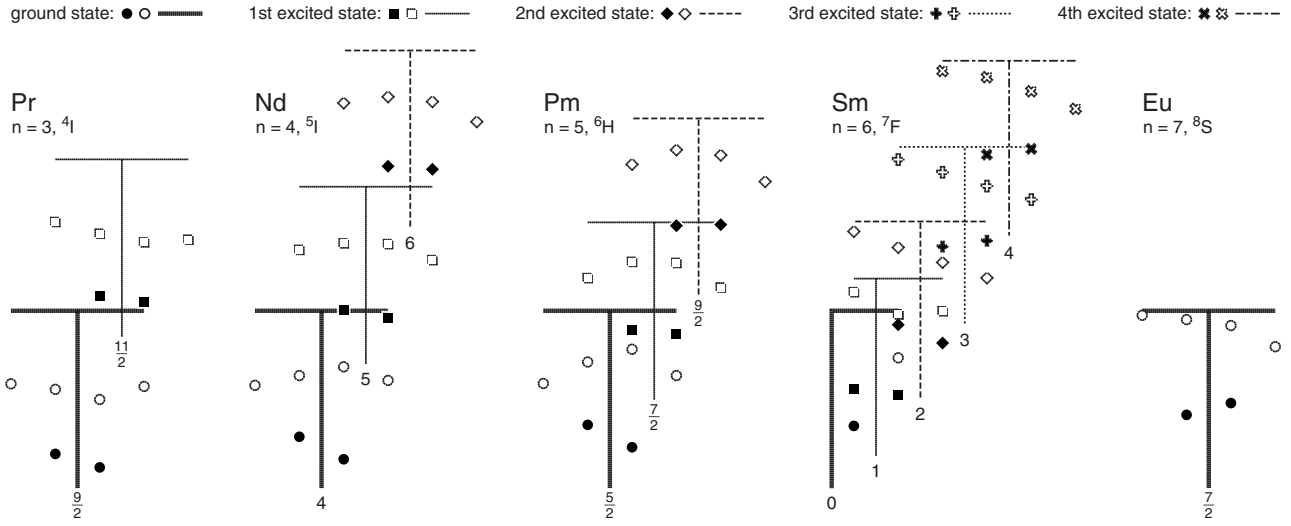


FIG. 1. Lanthanide anion $4f^n 6s^2 6p$ states relative to their $4f^n 6s^2$ neutral thresholds. Filled and open symbols represent $6p_{1/2}$ and $6p_{3/2}$ attachments, respectively. States are ordered with $J$ increasing to the right-hand side, and the vertical extension from each neutral threshold displays its $J$ and the energy scale (200 meV).

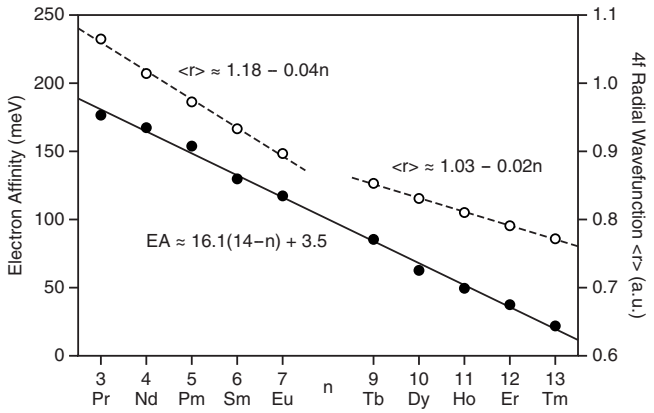


FIG. 2. Lanthanide anion $4f^n6s^26p$ EAs and $4f$ $\langle r\rangle$ vs $n$. The values for $\langle r\rangle$ are averages of $4f_{5/2}$ and $4f_{7/2}$ from the anion ground state $J$ ($\langle r\rangle$ of $4f_{7/2}$ is typically ~1% greater than that of $4f_{5/2}$).

$4f^3$ $j=15/2$ coupling which had small coefficients in the lowest levels of each $J$). In the data presented here there are two sets of virtual orbitals included in configurations with significant (>10 meV) correlation energies, whereas the older work had a single virtual orbital for each $l$. These current RCI calculations also include several second-order effects, such as $6s^2 \rightarrow nlvl' + vlvl'$ $(l'=l\pm 2)$ and $6s^26p \rightarrow 5d^2vp + 5d(vsvp + vpvd)$ which have zero interaction with $4f^36s^26p$ but do correlate other important configurations with large first-order energy contributions. Note also the absence in the earlier RCI values of BEs for the $6p_{3/2}$ attachments for $J=4$ and $J=5$, which are here slightly more bound than the $J=3$ and $J=6$ states. The increased relative binding of these states is due to the simultaneous optimization of both $6p_{1/2}$ and $6p_{3/2}$ attachments by the "swapping out" of the more compact one-electron radial wave functions as described in Sec. II A.

The $jj$ analysis of Table I is particularly useful in interpreting the wealth of bound states on the left-hand side of the lanthanide row. For each neutral threshold, we can generally identify two $6p_{1/2}$ attachments, one on either side of the neutral $J_n$ with $J=J_n\pm 1/2$. The $J$ with more possible attachments to higher thresholds is usually slightly more bound; $J_n+1/2$ on the left-hand side where the neutral energies increase with increasing $J$ and $J_n-1/2$ on the right-hand side where the ordering is inverted. The four possible $6p_{3/2}$ attachments with $J=J_n\pm 1/2$ and $J=J_n\pm 3/2$ typically lie ~100 meV above the $6p_{1/2}$ attachments, and the presence of attachments to higher thresholds again dictates to some degree the relative position of these four states.

The data for $Pr^-$ through $Eu^-$ are presented graphically in Fig. 1 along with additional states that lie above the ground states but are bound relative to their natural thresholds in the *ab initio* RCI calculations. Only data for neutral thresholds less than 300 meV above the ground state [13] are presented; there are an additional two levels of the lowest $LS$ term for each of Pr, Nd, and Sm as well as three more levels in Pm that are not shown. $Eu^-$ is perhaps the simplest case to illustrate the graphic representation of Fig. 1. The $4f^76s^2$ $J=7/2$ ground state is aligned vertically with the other lanthanide ground states, and the crossbar of the "T"-shaped

TABLE II. Examples of $\Delta E$ for possible strong $4f^n6s^26p \rightarrow 4f^n6s6p\epsilon p$ photodetachment channels from anion ground states. Where experimental $LS$ designations are available for these neutral thresholds [13], these channels obey the following selection rules: $\Delta J=\pm 1/2$, $\Delta L=0$, and $\Delta S=\pm 1/2$ (between anion states and neutral thresholds).

| Ion (−meV) | | Threshold ($cm^{-1}$) | | $\Delta E$ (eV) |
|---|---|---|---|---|
| $Pr^-$ $^5K_5$ | 177 | $^6K_{9/2}$ | 13433 | 1.842 |
| | | $^6K_{11/1}$ | 14178 | 1.934 |
| | | $^4K_{11/2}$? | 17578 | 2.356 |
| $Nd^-$ $^6K_{9/2}$ | 167 | $^7K_4$ | 13673 | 1.863 |
| | | $^7K_5$ | 14312 | 1.942 |
| | | $^5K_5$ | 20301 | 2.684 |
| $Sm^-$ $^8G_{1/2}$ | 130 | $^9G_0$ | 13796 | 1.840 |
| | | $^9G_1$ | 14000 | 1.866 |
| | | $^7G_1$ | 15651 | 2.070 |
| $Eu^-$ $^9P_3$ | 117 | $^{10}P_{7/2}$ | 14068 | 1.862 |
| | | $^8P_{5/2}$ | 15891 | 2.088 |
| | | $^8P_{7/2}$ | 15952 | 2.095 |
| | | $^8P_{5/2}$ | 21445 | 2.776 |
| | | $^8P_{7/2}$ | 21605 | 2.796 |
| $Tb^-$ $^7H_8$ | 85 | $J=15/2$ | 14888 | 1.931 |
| $Dy^-$ $^6H_{15/2}$ | 63 | $^7H_8$? | 15567 | 1.993 |
| $Ho^-$ $^5H_7$ | 50 | $^6H_{15/2}$? | 15855 | 2.015 |
| $Er^-$ $^4G_{11/2}$ | 38 | $^5G_6$? | 16321 | 2.061 |
| $Tm^-$ $^3D_3$ | 22 | $J=7/2$ | 16742 | 2.098 |

representation of this neutral state indicates the $J$ range (here $7/2\pm 3/2$) for possible $6p$ attachments to this level ($J$ increasing to the right). The vertical stroke of the "T" is labeled with the neutral threshold $J_n$ (7/2), and its vertical height (200 meV) indicates the energy scale of Fig. 1. The BEs are then plotted by $J$ with the symbol indicating the neutral core of each state and principle attachment type ($6p_{1/2}$ vs $6p_{3/2}$). Note that each point in Fig. 1 that lies below the level of the neutral ground states represents an anion state presented in the detailed analysis of Table I.

The gradual decrease in EA with increasing $n$ is clear in Fig. 1, but more important is the increased density of neutral thresholds ($2S+1$ levels for Pr through Sm). For Pr the first excited state ($^4I_{11/2}$) is high enough (~171 meV) that its $6p$ attachments (indicated by the square symbols) are unbound relative to the $^4I_{9/2}$ ground state. For Nd and Pm, $6p_{1/2}$ attachments to the first excited states (filled squares) are weakly bound relative to the ground state (one in $Nd^-$ and both in $Pm^-$, cf. Table I). For Sm, there are only two possible attachments to the $J_n=0$ ground state, but here the low-lying excited states result in additional bound states consisting of both $6p_{1/2}$ attachments to the first and second excited states as well as two of the $6p_{3/2}$ attachments to the first excited state. On the right-hand side of the lanthanide row (not shown graphically), the first excited states of the neutral are all over 300 meV above the ground state [13], and the in-

creased screening of the $4f^n$ electrons results in bound states only for the two $6p_{1/2}$ ground-state attachments. The $6p_{3/2}$ states for $Tb^-$, $Dy^-$, $Ho^-$, $Er^-$, and $Tm^-$ ($n=9$ to $n=13$) are unbound in these RCI calculations by averages of 15, 28, 45, 63, and 78 meV, respectively.

Considering the lowest bound state of each anion from Table I, we find a nearly linear decrease with $n$ for the lanthanide $4f^n6s^26p$ EAs as presented in Fig. 2. A similar relationship has long been known for BEs of $s$ attachments to $d^ns$ states in transition metal series [17]. Also shown in Fig. 2 are the $\langle r\rangle$ of the anion $4f$ one-electron radial wave functions, which also decrease nearly linearly with $n$, albeit with a slightly different slope on the left- and right-hand sides of the row. As $Z$ increases across the lanthanides, the effective charge within the $4f$ subshell radius also increases, since the $4f$ electrons provide little screening for one another. Each additional $4f$ electron thus results in a more compact subshell with increased screening for valence electrons and therefore less binding for the $6p$ attachment.

### B. Potential photodetachment channels

As suggested previously for $Nd^-$ [7], depending on the photon energy used in photodetachment studies, channels representing $6s\rightarrow\epsilon p$ may be much stronger (near $4f^n6s6p$ thresholds [13]) than the direct $6p\rightarrow\epsilon s+\epsilon d$ detachment to the neutral $4f^n6s^2$ ground states. In Table II we present potential channels from the anion ground states which leave the neutral atom in excited states that would obey the electric dipole selection rules. Since $6s\rightarrow\epsilon p$ "carries" these selections rules, the remainder of the anion state must match the neutral threshold *JLS*, which is possible for anion-neutral combinations with the same $L$ and differences of $\pm 1/2$ in $J$ and $S$.

As mentioned previously, accurate photodetachment cross-section calculations are potentially an order of magnitude more difficult than the *ab initio* BE calculations presented here; these neutral threshold are 10–20 levels up in the spectra for each $J$, usually above other manifolds with $4f^{n-1}$ subgroups [13], and there are potentially hundreds of individual partial cross sections required for photodetachments from each anion bound state. Proper positioning and mixing of $4f^n6s6p^2$ resonances [7] would also be required (the selection rules would suggest large impact on the cross sections for resonances with the $4f^nls$ matching the neutral ground state $LS$ and $6s6p^2$ dominant $ls$ terms of $^2S$, $^2P$, and $^2D$).

The intent of Table II is to provide approximate energies for potentially prominent features in experimental data, and hopefully future analysis of these data can be used to adjust the *ab initio* BEs presented here, e.g., as mentioned in Sec. I, identification of a channel from the anion ground state could be used to shift the excited bound states by the same correction. Thorough analyses of experimental spectra may also require improvements in identification of thresholds, since in most cases only the lowest few $4f^n6s6p$ states are currently labeled [13]. We also suggest that investigators interested in studying direct photodetachment to lanthanide ground states should use incident photon energies well below the $\Delta E$s presented in Table II to avoid complications of the near threshold $6s\rightarrow\epsilon p$ detachments.

### C. Conclusions and future work

Our methodology of *jls* restrictions on $4f^n$ subgroups in the lanthanides has been tested in the simpler cases ($Pr^-$ and $Nd^-$) and shown to produce negligible energy losses compared to calculations with more thorough bases, e.g., the energy difference in each neutral ground state after applying the improved *jls* rotation and restriction is less than 10 $\mu$eV. The algorithm has been successfully extended to the middle of the lanthanide row where the complexity of the systems would otherwise make inclusion of similar amounts of correlation prohibitively expensive. While the errors due to treating the $4f$ subshells as corelike are difficult to estimate, it is encouraging that RCI calculations with the equivalent correlation predict no bound states for $Yb^-$ (the $6p_{1/2}$ and $6p_{3/2}$ attachments to $4f^{14}6s^2$ $J=0$ are unbound by 2 and 91 meV, respectively), in agreement with more recent experimental [18] and computational [19] results.

Prior to our use of these algorithms, no computational values were available for lanthanide anion BEs for $Nd^-$ ($n=4$) to $Er^-$ ($n=12$). The nearly linear relationship for the lanthanide EAs as shown in Fig. 2 represents a significant step forward in the understanding of these complex systems that previously could not be appreciated given just the $Pr^-$ ($n=3$) [15] and $Tm^-$ ($n=13$) [16] ends of this range. We hope that the predicted relative simplicity of the $6p$ attachments on the right-hand side of the row (two bound states for each anion, both of which is bound by nearly the same energy) encourage further experimental interest in these systems. Specifically, investigations involving the suggested channels of Table II in just two or three of these systems could use this predicted linear trend to rescale and improve all the BEs presented here, including the more complex systems on the left-hand side of the row.

The next step in our survey of the lanthanide anions BEs is to consider $4f^m5d6s^2$ neutral thresholds, which will require four-electron valence subgroups in the anion $6p$ attachments. Data already prepared for the creation of $4f^n6s^26p$ anion basis functions will be easily reused in the $4f^m5d6s^2$ neutral calculations, but data for four-electron subgroups with various $j$ restrictions must be created independently. Due to differing occupancy of the $4f$ subshell ($m=n-1$, resulting in less screening), one might expect that $6p$ attachment to the Gd ($m=7$) ground state is likely to produce an EA greater than the trend presented in Fig. 2. In fact, the corresponding $Ce^-$ $6p$ attachment to $4f5d6s^2$ is predicted in our earlier RCI calculations [6] to be $\sim$100 meV more bound than the linear extrapolation from Fig. 2 (EA $\sim$197 meV if the Ce ground state were actually $4f^26s^2$ rather than $4f5d6s^2$). Interestingly, a similar difference in $4f$ screening for $4f^85d6s^2$ vs $4f^96s^2$ could potentially result in $6p$ attachments to the low-lying first excited state of Tb [13] being more bound than the attachments to the ground state which are presented here.

Finally, given our improvements over the earlier $Pr^-$ RCI calculations [15], we have made a few preliminary calcula-

tions for 6*s* attachments to the excited $4f^25d^26s\ ^6L_{11/2}$ state at 6714 $cm^{-1}$ [13]. While this state was earlier found to be unbound [15] relative to the Pr ground state, a weakly bound $4f^25d^26s^2$ state that also photodetaches to the excited $^6L_{13/2}$ state at 7630 $cm^{-1}$ [13] might account for the double peak seen in the experimental spectra [1] (splittings of 114 vs 96 meV). These $Pr^-$ calculations will also require detailed data for four-electron subgroups to be included in this methodology (though savings in basis size by applying it to a $4f^2$ subgroup will be fairly modest).

## ACKNOWLEDGMENTS

Support for this work from the National Science Foundation, Grant No. PHY-0097111, is gratefully acknowledged.

[1] V. T. Davis and J. S. Thompson, J. Phys. B **35**, L11 (2002).
[2] V. T. Davis and J. S. Thompson, J. Phys. B **37**, 1961 (2004).
[3] V. T. Davis and J. S. Thompson, Phys. Rev. A **65**, 010501(R) (2001).
[4] V. T. Davis, J. S. Thompson, and A. Covington, Nucl. Instrum. Methods Phys. Res. B **241**, 118 (2005).
[5] M. J. Nadeau, M. A. Garwan, X. L. Zhao, and A. E. Litherland, Nucl. Instrum. Methods Phys. Res. B **123**, 521 (1997).
[6] S. M. O'Malley and D. R. Beck, Phys. Rev. A **74**, 042509 (2006).
[7] S. M. O'Malley and D. R. Beck, Phys. Rev. A **77**, 012505 (2008).
[8] S. M. O'Malley and D. R. Beck, J. Phys. B **38**, 2645 (2005).
[9] S. M. O'Malley and D. R. Beck, Phys. Rev. A **70**, 022502 (2004).
[10] U. Fano, Phys. Rev. **124**, 1866 (1961).
[11] F. H. Mies, Phys. Rev. **175**, 164 (1968).
[12] P. G. Burke and K. A. Berrington, *Atomic and Molecular Processes: An R-Matrix Approach* (Institute of Physics, Bristol, Philadelphia, 1993).
[13] *Atomic Energy Levels—The Rare-Earth Elements*, edited by W. C. Martin, R. Zalubas, and L. Hagan, Natl. Bur. Stand. Ref. Data Ser. Natl. Bur. Stand. (U. S.) Circ. No. 60 (U.S. GPO, Washington, DC, 1978).
[14] J. P. Desclaux, Comput. Phys. Commun. **9**, 31 (1975).
[15] K. Dinov and D. R. Beck, Phys. Rev. A **51**, 1680 (1995).
[16] J. A. Chevary and S. H. Vosko, J. Phys. B **27**, 657 (1994).
[17] C. S. Feigerle, R. R. Corderman, S. V. Bobashev, and W. C. Lineberger, J. Chem. Phys. **74**, 1580 (1981).
[18] H. H. Andersen, T. Andersen, and U. V. Pedersen, J. Phys. B **31**, 2239 (1998).
[19] E. N. Avgoustoglou and D. R. Beck, Phys. Rev. A **57**, 4286 (1998).